Fast Response Photoconductive for Fe_3O_4:Ce Nanoparticles

Iftikhar M. Ali[1] , Safaa Abbas[2]

[1] Dept. of phys., College of science, Baghdad University. iftikhariq@gmail.com

[2] Dept. of phys., College of science, Baghdad University. Alzaidysa4@gmail.com

Abstract

Fe_3O_4:Ce thin films were deposited on glass and Si substrates by Pulse Laser Deposition Technique (PLD). Polycrystalline nature of the cubic structure with the preferred orientation of (311) are proved by X-ray diffraction. The nano size of the prepared films are revealed by SEM measurement. Undoped Iron oxide and doped with different concentration of Ce films have direct allowed transition band gap with 2.15±0.1 eV which is confirmed by PL Photoluminescence measurements. The PL spectra consist of the emission band located at two sets of peaks, set (A) at 579±2 nm , and set (B) at 650 nm, respectively when it is excited at an excitation wavelength of 280 nm at room temperature.

I-V characteristics have been studied in the dark and under various illuminations intensities. Ideality factor, barrier height and saturation current have been calculated in the dark. Photocurrent, gain and sensitivity have been measured under illuminations with halogen lamp with different intensities. Fe_3O_4:Ce thin films have been used in photoconductive applications, many wavelengths have been used; 373, 395, 445, 475, 540, 935 nm. Sensitivity, rise and fall times have been calculated for these wavelengths. In general the results revealed fast rise and fall times which is~ ms with more than 1000% sensitivity for 935 nm.

Key words: Fe_3O_4; photoconductivity; structural properties; optical properties, responsivity.

Introduction

The doped nanomaterials have been largely studied in recent years due to their widespread applications in various devices such as sensors, solar cells, lasers, photocatalysts, photodetectors, IR detectors, optical communication, colour television, flat panel display, phosphors, light emitting diodes, etc. [1–6]. Fe_3O_4 is one of the important materials with the band gap of 2 eV. It is transparent in the visible spectral region. Induced sub-band gap transitions in Fe_3O_4 occur at energies in the visible range that allows the optical detection of traps, radiative recombination centers and surface states. The emission properties of Fe_3O_4 are frequently being used in solid-state photoluminescence (PL) and electroluminescence studies related with the mechanism of emission in semiconductors. In addition, the small size and high optical activity of Fe_3O_4 nanoparticles (NPs) make them interesting for optoelectronic applications operating in the NIR region.

This paper deals with the photoconductivity (PC) properties of Ce doped Fe_3O_4 nanoparticles. Photoconductivity is considered to be an important tool for providing information regarding the nature of the photo-excitations. Since last decade the photoconductive properties of the inorganic nanoparticles have become subject of intensive study [7]. Not only because of fundamental interests in the nature of the electronic excitations but also due to their applications in wide range of optical and electronic devices. In semiconductors, PC generally arises due to generation of electron–hole pairs because of the interaction of photons with bound electrons of lattice atoms. The conductivity of material depends upon the carrier density and complex process of carrier generation, trapping, and recombination [8].

A good photoconductive device requires not only efficient charge separation but also efficient transport of charge carriers to electrode [9]. In this paper we report X-ray diffraction (XRD), SEM and PC results of Ce doped Fe_3O_4 nanoparticles synthesized by PLD technique. Dark-conductivity and photoconductivity measurements are taken at low voltage. The sensitivity was taken under some wavelength light exposure. The rise time and fall time have also been calculated under these

conditions. There is perhaps no report on photoconductivity of Ce doped Fe_3O_4 nanoparticles. The objective is to see if there is any change in behavior with the doping with Ce ions in host Fe_3O_4 NPs.

Experemental Procedure

Before starting the deposition, the solutions according to the films components was mixed then put it on the magnetic stirrer to be sure that the mixture solutions are mixed properly and to get solution to deposition on the silicon wafer and glass substrates were cleaned. After that, the powder compress by compressor at pressure (4 ton) when it finish can start the deposition process inside PLD chamber at 600 mJ and 250 pulses with 6Hz pulse width, The distance between the pill and the substrate was fixed at 2 cm.

The X-ray diffraction (XRD) spectra of the films were obtained to verify their crystal structure using a (Cu-Kα) radiation with λ = 0.154 nm. Optical transmission data were obtained using UV-Vis spectrometer at wavelengths ranging from 400 nm to 900 nm. Scanning electron microscopy (SEM) is employ to know the grain size of material and to observe the surface morphology of the films.

Results and Discussion

1- X-ray diffraction analysis for Fe_3O_4 powders:

Figure 1 shows the XRD patterns of the undoped and Ce-doped Fe_3O_4 nanoparticles. Samples exhibited a FCC phase. The sharp peaks in these structures indicated that the materiales were highly crystallized. All the peaks of XRD patterns were analyzed and indexed using ICDD data base, comparing with standards. It can be noticed from X-ray patterns that the peak positions at (2θ=30.0555, 35.4495, 43.1077, 53.4961, 57.0255 and 62.6193) referred to (202), (311), (400), (422), (333), (404) plane directions, respectively. Strongest peak occurs for the (311) plane at 2θ=35.4495 [Card No. (# 96-900-6195)] which represents the preferred orientation. The analysis of the diffraction patterns showed the formation of a cubic spinel structure, due to the strongest reflection that proceeds from the (311) plane. At doping, the increase in the (311) peak may be attributed to the formation of new nucleating centers due to the dopant atoms resulting from the decrease of nucleation energy barrier [6]. Crystallite size was determined from the full-width at half maximum (FWHM) of peak, using the Scherrer approximation, which assumes the small crystallite size to be the cause of line broadening equation 1. The average crystallite size was estimated through XRD analysis. This size was found to be (31.3 nm), making the produced, at a first glance, suitable for technological applications this refer to decreasing the size with doping, which leads to increasing quantum confinement as shown in Table 1. In this case the inoculation type is interstitial because no peaks corresponding to cerium element were observed, demonstrating that Ce ions are dispersed in Fe_3O_4 matrix. Also no peaks corresponding to other impurities were identified in the patterns, indicating the high purity of the final product.

$$D = K \lambda / \beta \cos \theta \qquad (1)$$

where λ is the X-ray wavelength (1.54Å), β is full width at half maximum (FWHM), θ is Bragg's angle, K is the Scherrer's constant ≈ was ranged from (0.9 to 1) depends on geometry of structure.

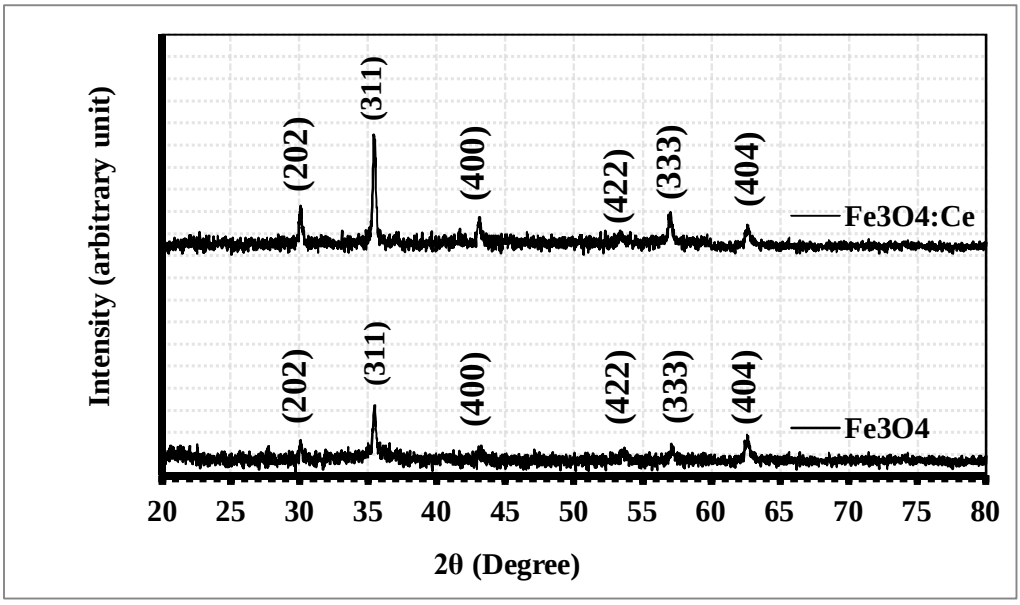

Figure 1. XRD patterns of as deposited undoped and Ce doped Fe_3O_4

Table 1 Structural parameters of undoped and Ce-doped Fe_3O_4 nanoparticles.

Sample	2θ (Deg.)	FWHM (Deg.)	d_{hkl} Exp.(Å)	Crystallite size (nm)	d_{hkl} Std.(Å)	(hkl)	Phase	Card No.
Fe_3O_4	30.1221	0.3330	2.9644	24.7	2.9688	(202)	Fe_3O_4	96-900-6195
	35.4495	0.2664	2.5302	31.3	2.5318	(311)	Fe_3O_4	96-900-6195
	37.1143	0.3996	2.4204	21.0	2.4240	(222)	Fe_3O_4	96-900-6195
	43.0411	0.5993	2.0999	14.3	2.0993	(400)	Fe_3O_4	96-900-6195
	53.5627	0.6660	1.7095	13.4	1.7140	(422)	Fe_3O_4	96-900-6195
	57.0921	0.5994	1.6120	15.1	1.6160	(333)	Fe_3O_4	96-900-6195
	62.6193	0.4662	1.4823	20.0	1.4844	(404)	Fe_3O_4	96-900-6195
Fe_3O_4:Ce	30.1221	0.2664	2.9644	30.9	2.9688	(202)	Fe_3O_4	96-900-6195
	35.3829	0.2664	2.5348	31.3	2.5318	(311)	Fe_3O_4	96-900-6195
	37.1143	0.4662	2.4204	18.0	2.4240	(222)	Fe_3O_4	96-900-6195
	43.1743	0.4661	2.0937	18.3	2.0993	(400)	Fe_3O_4	96-900-6195
	53.4295	0.7325	1.7135	12.1	1.7140	(422)	Fe_3O_4	96-900-6195
	56.8923	0.3330	1.6171	27.1	1.6160	(333)	Fe_3O_4	96-900-6195
	62.6193	0.5994	1.4823	15.5	1.4844	(404)	Fe_3O_4	96-900-6195

2- Scanning electron microscopy (SEM):

The surface morphologies of pure Fe_3O_4 and doped with cerium for films have been investigated using scanning electron microscopy (SEM) and figures 2(a, b) show the SEM of thin films samples. As shown in figure 2, the SEM images indicated that the Fe_3O_4 nanoparticles had a diameter less than 100 nm, which proves the nano size for the prepared films.

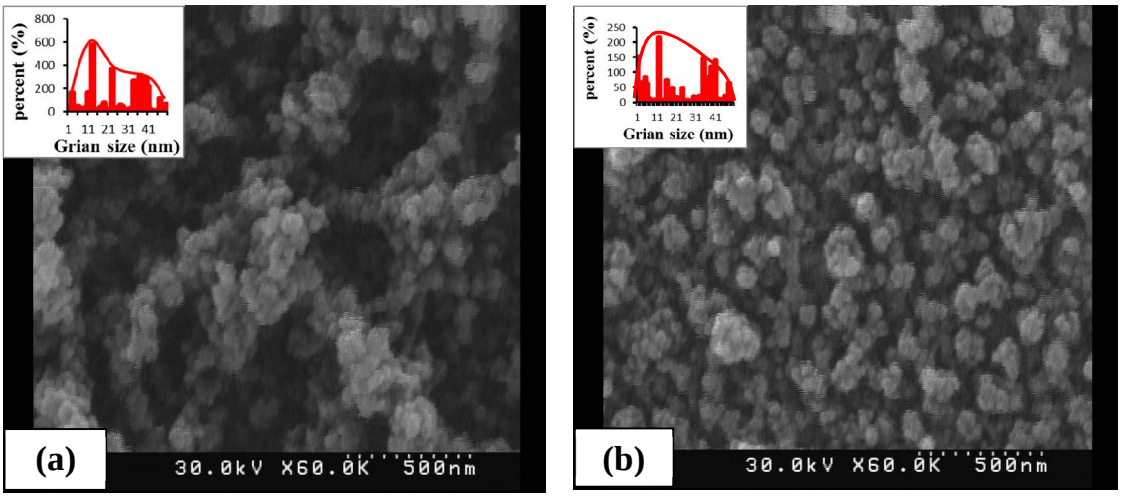

Figure 2 SEM images for (a) Fe_3O_4 and (b) Fe_3O_4:Ce thin films.

Optical Measurements:

a- Optical Energy Gap (E_g):

Optical Measurements for pure and doped Fe_3O_4 with cerium is carried out in the wavelength range (480–1100) nm. The optical energy gap (E_g) value can be determined by applying Tauc relation. The drawing between $(\alpha h\upsilon)^2$ on the Y-axis and photon energy ($h\upsilon$) on the X-axis and from the cross tangent curve with ($h\upsilon$) axis, this cross point represented the energy gap value, which denoted by Tauc plot. Figure 3 shows the determination of the direct energy gap value for the pure Fe_3O_4 and doped with cerium, it can be noticed that with doping energy gap will increase [see Table 2] that means the grain size decreasing, so we have blue shift, which related to the size decrease of particles and is attributed to increasing quantum confinement, resulting in a more discrete energy spectrum of the individual nanoparticles [10].

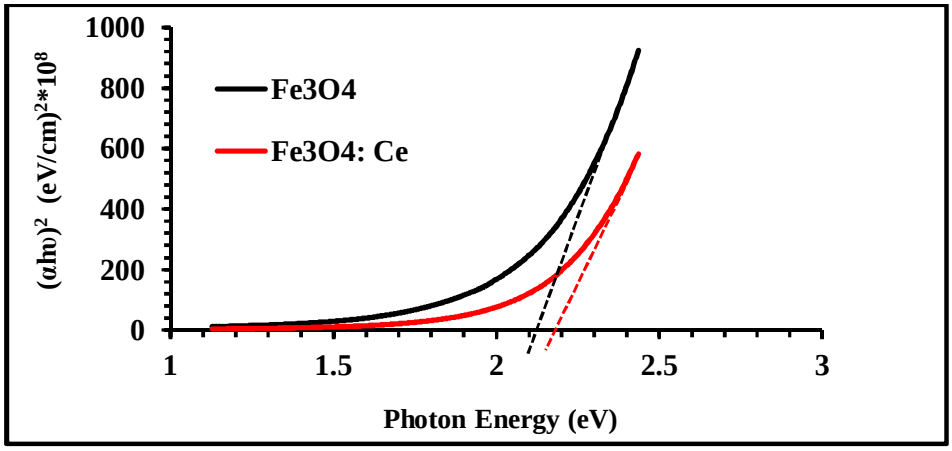

Figure 3 Tauc plot for pure and doped Fe_3O_4 with Ce

The effect of the quantum confinement on impurity depends upon the size of the host crystal. As the size of the host crystal decreases, the degree of confinement and its effect increases and this agrees with many researchers such as [7, 8, 9]. Optical energy gap results matches with XRD results that the grain size decreases with doping.

Table 2 Energy gap calculated from UV-Vis spectra

Sample	E_g (eV)
Fe_3O_4	2.14
Fe_3O_4:Ce	2.18

Electrical measurement

a- Hall Effect:

Concentration (n_H), Hall mobility (μ_H) and type of conductivity have been estimated from Hall measurements for pure Fe_3O_4 films and doped with Ce which were deposited on glass substrates. The values of carrier concentration (n_H) and Hall mobility (μ_H) were calculated using equations (2) and (3). The variation of carriers concentration (n_H) and Hall mobility (μ_H) of pure Fe_3O_4 and doped with Ce thin films are shown in Table 3.

$$R_H = \frac{1}{n.q} \qquad \text{…….. (2)}$$

$$\mu_H = \sigma |R_H| \qquad \text{…….……(3)}$$

where σ is the electrical conductivity calculated by the equation:

$$\sigma = L / R*A \qquad \text{…….. (4)}$$

L is a distance between electrodes, R is resistance of a sample at room temperature, A is area for electrode.

Table 3: Hall measurements results of Fe_3O_4 thin films

Sample	$n_s(cm^{-2})$ $*10^5$	$\mu_H(cm^2/V.s)$ $*10^2$	type
Fe_3O_4	3.13	55	P
Fe_3O_4:Ce	10.3	21.1	P

b- Photoconductivity Measurements:

1) I-V Characteristics:

The current-voltage (I-V) characteristics of the fabricated device are illustrated in figure 4 for pure and doped Fe_3O_4. The measurements have been done in the dark and under illumination with different light intensities (1710, 965, 652) mW/cm^2 from Halogen lamp. From this figure, one can observe that with doping there is increasing in photo current and at high light intensities, the relation between current and voltage varies from shottcky (nonlinear relation) to ohmic (linear relation), that means more concentration of charge carriers transit within metal-semiconductor interface, so there is no barrier height in front of the carriers.

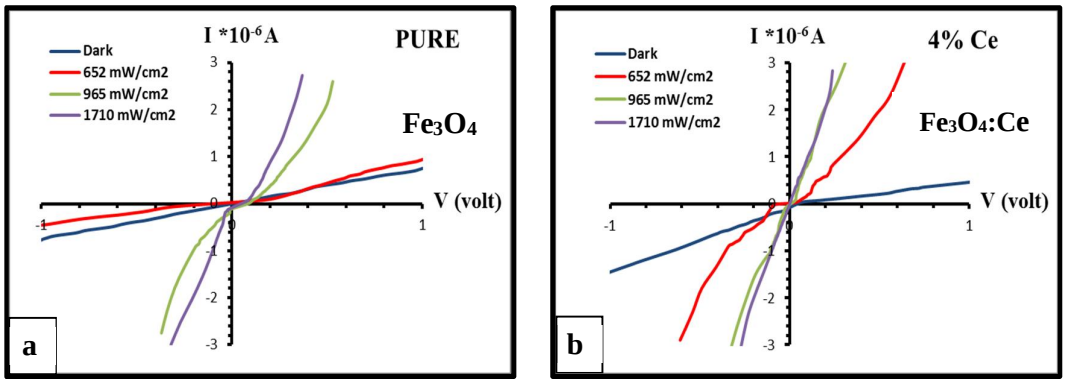

Figure 4. I-V characteristics in the dark and under illumination with different intensities for (a) pure Fe_3O_4 and (b) Ce doped Fe_3O_4.

i) I-V Characteristics in the Dark:

In general forward dark current is generated due to the flow of majority carriers and the applied voltage injects majority carriers which leads to the decrease of the built – in potential, as well as the width of the depletion layer. As the majority and minority carrier concentration is higher than the intrinsic carrier concentration ($n^2_i < np$) which generate the recombination current at the low voltage region (0-0.08) Volt as seen in figure 5. This is because the excitation of electrons from valence band (V.B) to conduction band (C.B) will recombine with the holes which are found at the V.B., and this is observed by the little increase in recombination current at low voltage region [6]. While the tunneling current occurs at the high voltage region (>0.08) Volt respectively. After that there is a fast exponential increase in the current magnitude with increasing of the voltage and this is called diffusion current, which dominates [6].

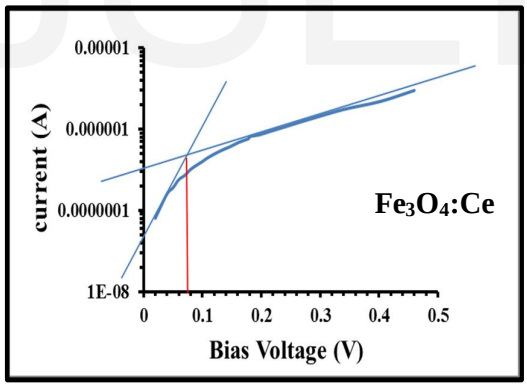

Figure (5): I-V characteristics in the dark for Fe_3O_4:Ce.

The reverse bias current also the same case of forward bias current. Also we can observe from Table 3 that the value of the saturation current decreases with doping which is attributed to evolving defects and dislocations that have an effect on the mobility of charge carriers. Also these defects evolutions allow energy levels to be within the energy gap, these defects are within the depletion region and act as active recombination centers, and consequently they decrease current flow across the junction. The value of saturation current I_s, ideality factor n and barrier height Φ_{Bn} are calculated from equations (5) and (6) [10], and their values are listed in Table 3.

$$\Phi_{Bn} = (k_B T/q)\, Ln(AA^* T^2/I_s) \quad \ldots\ldots\ldots\ldots\ldots\ldots\ldots\ldots (5)$$

$$n=q/k_BT\ (V/Ln(I_F/I_S)) \text{ ..……..……..…(6)}$$

Table (3) I_s, n, Φ_{Bn}, rise time, fall time and height barrier values for pure Fe_3O_4 and doped with cerium at dark.

Sample	I_s*10^{-8} (A)	n	%S	t_r (sec)	t_f (sec)	Φ_{Bn} (eV)
Fe_3O_4	4.5	8.94	67	0.802	0.81	0.514
Fe_3O_4:Ce	1.5	3.752	960	0.811	0.809	0.542

2) R-t Characteristics:

The resistance-time (R-t) characteristics are taken with the following wavelengths (370, 395, 445, 473, 531 and 935) nm with intensities (100, 581, 479, 446, 2396 and 8.06) nW/cm^2 respectively. Figures from (6) to (12) show the photo response for devices with time. Also Table 4 shows the sensitivity for pure Fe_3O_4 and doped with cerium. As for (370 and 395) reaches to maximum value at (6 and 8) %Ce, respectively after that decrease. Also they increase sensitivity themselves with increasing wavelength until reaching to maximum value for sensitivity (1044%) at (4%) Ce at wavelength (935 nm) of intensity (8.06 nw/cm^2) which is in IR spectrum region. When the light was turned on, resistance decreased and after the light was turned off, the resistance returned to its original value. This process was repeated many times as seen from figure (6) to (12) and the rise and fall times in this process are < 1 sec for each state turn (on or off). From our data, it appears that is possible to control the response of the current in a semiconducting photo sensor because the electrons in the nanoparticles receive their excitation energy from the power of the light source, it is possible to "switch" these nanoparticles reversibly between higher and lower states of conductivity. From (R-t) figures, one can conclude that with doping the sensitivity is higher than that without doping. This giant enhancement in photo conductance was attributed to the energy levels introduced by the dopant atoms lying in the corresponding band gap of Fe_3O_4. Such states served as "hopping" states and increased the excitation probability of an electron to the conduction band.

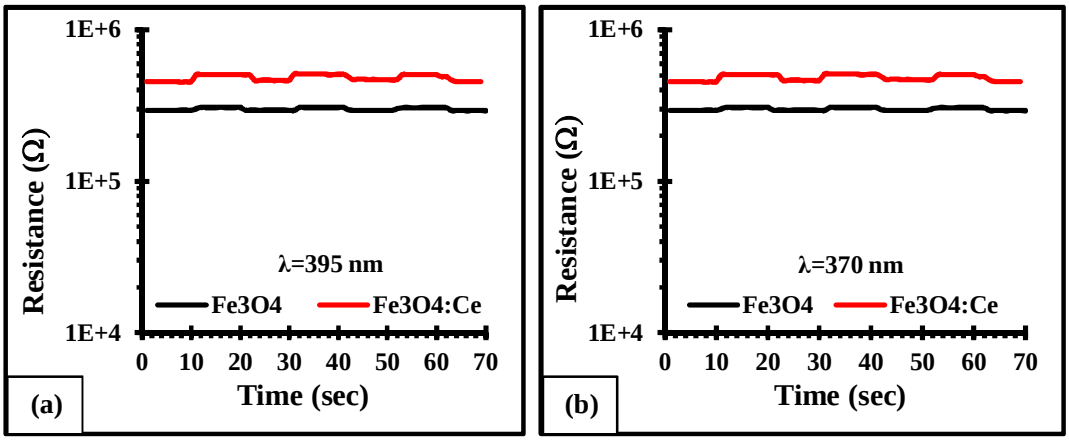

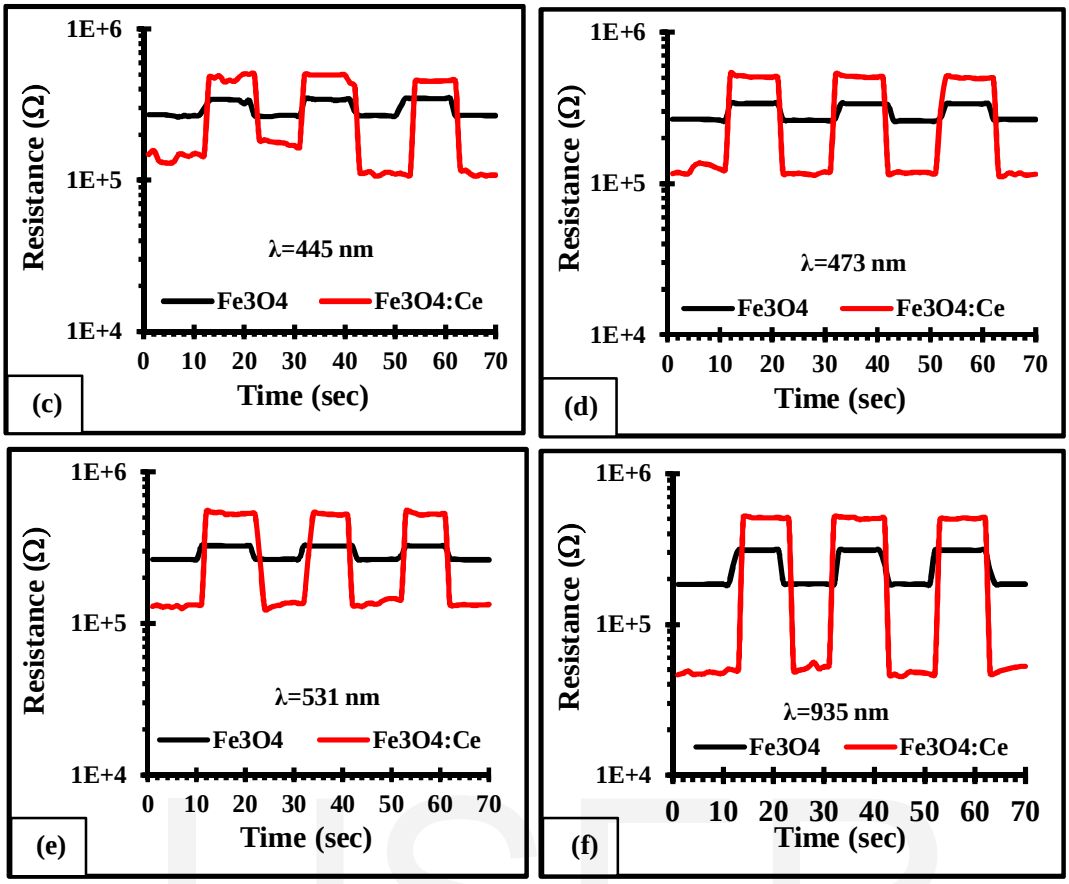

Figure 6. Comparison of Photo response time of the fabricated photo sensor between pure and Ce doped Fe_3O_4 upon exposure to (a) 380 nm, (b) 395 nm, (c) 445 nm, (d) 473 nm, (e) 531 nm, (f) 930 nm.

Table (4) The sensitivity as a function of wavelength for pure Fe_3O_4 and doped with Ce.

Sample	370 nm	395 nm	445 nm	473 nm	531 nm	935 nm
Fe_3O_4	2	4.31	28.36	29.27	23.02	67.25
Fe_3O_4:Ce	5.53	9.14	351.06	345.3	333.5	1044.17

From (R-t) figures, one can note that the resistance decreased sharply upon exposure to IR light, and then exhibited hill-like behavior reaching the steady state. This behavior could be attributed to deep level defect that exist in the Fe_3O_4:Ce lattice which served as traps for photo generated electrons [7].

Conclusion

Pure and cerium doped iron oxide thin films have been prepared successfully by PLD technique. XRD proved that the prepared iron oxide is Fe_3O_4 phase with (311) preferred orientation plane. SEM measurements proved the nanosize of the prepared thin films. Photo conductive sensor has been successfully fabricated from the prepared nano material. Many wavelength have been used to examine our device, higher sensitivity ~ 1000% at 935 nm and very fast response time ~ ms for small

amount of cerium without any bias voltage, making them having potential applications as electrical gating for binary switching without necessary electric powder.

References

[1] G. Neri, "Metal oxide nanostructures for solid state gas sensors: A Recent patent survey", Recent patents on Materials Science, Vol. 4, PP. 146-158, (2011).

[2] Yamazoe,N. Toward innovations of gas sensor technology. *Sens. Actuat. B Chem.* 108, 2–14. (2005).

[3] Cao,C.Y., Qu,J., Yan,W.S., Zhu, J.F.,Wu, Z.Y., and Song,W.G. Low-costsynthesisofflow- erlike α-Fe_2O_3nanostructures for heavy metal ion removal :adsorption property and mechanism. *Langmuir* 28, 4573–4579 (2012).

[4] Li, H.,Li,W.,Zhang,Y.,Wang,T., Wang,B.,Xu,W., Chrysanthemum-like[small alpha]-FeOOH microspheres produced by a simple green method and their outstanding ability in heavy metal ion removal. *J. Mater. Chem.* 21, 7878–7881(2011).

[5] Sadik, O.A., Wanekaya,A.K., and Andreescu,S. Advances in analytical technologies for environmental protection and public safety. *J. Environ.Monit.* 6, 513–522 (2004).

[6] Kawamura,K.,Kerman,K.,Fujihara, M., Nagatani,N.,Hashiba,T.,and Tamiya,E. Development of a novel hand-held formaldehyde gas sensor for the rapid detection of sick building syndrome. *Sens.Actuat.BChem.* 105, 495–501(2005).

[7] Akyildiz,I.F., and Kasimoglu,I. H. Wireless sensor and actor networks :research challenges. *Ad HocNetw.* 2, 351–367 (2004).

[8] C. Domingo,R. Rodriguez-Clemente, and M. Blesa, "*Morphological properties of α-FeOOH, γ-FeOOH and Fe3O4 obtained by oxidation of aqueous Fe(II) solutions*", J. Colloid Interf. Sci. 165, pp. 244-252 (1994).

[9] A. Ishizumia, C. W. Whiteb and Y. Kanemitsu, "Photoluminescence properties of impurity-doped ZnS nanocrystals fabricated by sequential ion implantation", Physica E, 26, 24–27 (2005).

[10] Ruiz,A.M.,Sakai,G.,Cornet,A., Shimanoe, K.,Morante,J.R.,and Yamazoe,N.Cr-dopedTiO2 gas sensor for exhaust NO2 monitoring. *Sens.Actuat.BChem.* 93, 509–518 (2003).